Metal Atoms and Particles on Oxide Supports: Probing Structure and Charge by Infrared Spectroscopy

Martin Frank, Marcus Bäumer,* Ralf Kühnemuth,† and Hans-Joachim Freund

Fritz-Haber-Institut der Max-Planck-Gesellschaft, Faradayweg 4-6, D-14195 Berlin, Germany

Received: February 26, 2001; In Final Form: June 27, 2001

Supported metal particles may exhibit properties fundamentally different from the corresponding bulk materials. To gain insight into principles underlying size- and structure-dependent phenomena, a structural characterization of small aggregates at the atomic level is crucial, while far from straightforward. A long-standing question in the study of supported clusters and metal-oxide interfaces concerns the extent of metal-oxide charge transfer. We show that infrared spectroscopy, utilizing carbon monoxide as a probe molecule, may provide valuable information on both structure and charge of ultrasmall metal aggregates and single metal atoms. To create supported particles containing only few atoms or even a single atom, submonolayer amounts of the transition metals palladium, rhodium, and iridium were vapor-deposited onto a thin, well-ordered alumina film at low substrate temperatures. Scanning tunneling microscopy served to characterize nucleation behavior and average particle size. Sharp, discrete features in the infrared spectra of adsorbed CO are due to uniform metal (M) carbonyls, most notably the mono- and dicarbonyl species MCO and $M(CO)_2$. The thermal behavior of such carbonyls is reflected in the thermal evolution of their infrared signatures. Comparing the C−O stretching frequencies of MCO species on the aluminum oxide film to those of their matrix-isolated neutral and charged counterparts, the charge of the metal centers is estimated. In this way, the extent of metal-oxide charge transfer at point defects and regular sites of the alumina film is shown to be smaller than ±0.2 elementary charges. By contrast, Rh atoms more strongly bound to oxide line defects are oxidized by the alumina substrate.

1. Introduction

Nanoparticles, objects in the borderland between single atoms and the solid state, may exhibit surprising size-dependent physical and chemical properties. Whereas bulk Rh, for example, is paramagnetic, small Rh particles exhibit ferromagnetism.[1] And while bulk Au is unreactive at room temperature, Au particles with diameters below 5 nm have been shown to be catalytically active.[2] Possible applications of small particles range from magnetic storage across nanoelectronics and photonics to heterogeneous catalysis. These applications mostly rely on such objects supported on or embedded in an insulating solid. This insulating material is often an oxide.[3]

As illustrated by the examples of Rh and Au, the geometric structure of small aggregates, their electronic properties, and their reactivity are intimately correlated. In fact, it has been shown that even changes in the size of supported particles by a single atom may drastically alter their properties.[4,5] To establish such connections, a detailed characterization of particle structure is clearly desirable. For the structural investigation of small particles in a solid environment, a number of experimental techniques are at hand. Three-dimensional samples may be studied by, e.g., transmission electron microscopy (TEM),[6] X-ray diffraction,[7] or extended X-ray absorption fine structure.[8] For studies of particles supported on planar surfaces, also surface science methods, such as scanning tunneling microscopy (STM), atomic force microscopy, high-resolution electron diffraction, or photoelectron diffraction may be utilized.[9]

However, in the regime of objects consisting of single or few atoms, their detection and structural characterization is far from straightforward. In many cases, such particles are not present in sufficient concentration to provide an intense diffraction pattern or sizable spectral signatures. TEM is capable of resolving atomic details of larger particles, but often fails to detect objects below about 1 nm in diameter.[6] By contrast, much smaller objects and even single adatoms may routinely be detected by STM, rendering morphological information on nucleation and growth accessible. Yet the diagnosis of particle structure at the atomic level is not a simple task, as STM image formation results from a complex interplay between the geometric and electronic properties of substrate, particle, and tip.[10] To enable the study of oxide-supported particles by STM, conducting oxides[11−16] and thin isolator films on metal substrates[17−19] have been utilized as a support. For such oxide samples, image formation is even more complex than for metal-on-metal systems.[13] Atomically resolved STM images of individual oxide-supported particles containing *a small number of atoms* are therefore extremely rare.[16] On larger crystallites, atomic resolution has occasionally been attained.[12,15,20]

In this article, we show that vibrational spectroscopy may be a valuable tool to study ultrasmall metal particles and single metal atoms. To this end, we vapor-deposited small amounts of transition metals onto a thin alumina film grown on a NiAl single crystal surface under ultrahigh vacuum (UHV) conditions. The nucleation of small, individual metal particles was verified by STM. We then observed the vibrations of adsorbed probe molecules by infrared reflection absorption spectroscopy (IRAS). As a probe molecule, we utilized carbon monoxide, which possesses a large dynamic dipole moment and, consequently, a

* Corresponding author. Fax: +49-30-8413-4101. E-mail: baeumer@fhi-berlin.mpg.de.

† Present address: Max-Planck-Institut für biophysikalische Chemie, Am Fassberg 11, D-37077 Göttingen, Germany.

10.1021/jp010724c CCC: $20.00
Published on Web 08/16/2001

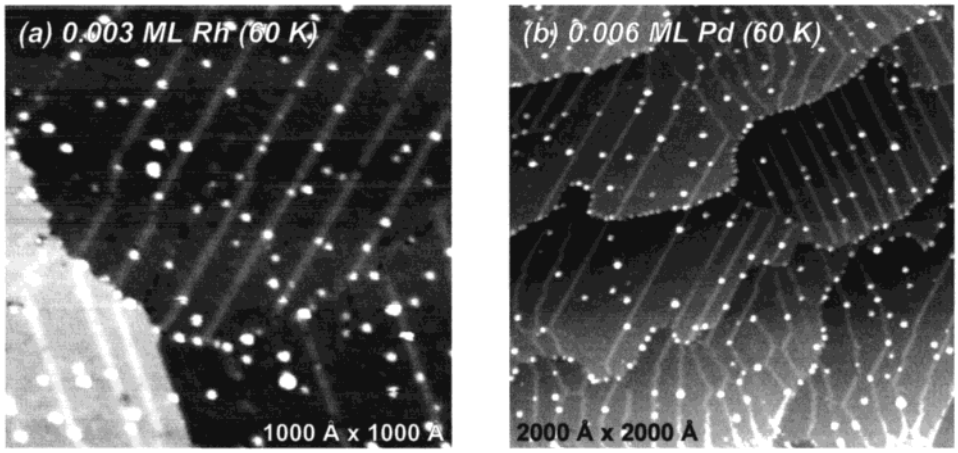

Figure 1. Room-temperature STM images recorded after deposition of very small amounts of Pd and Rh onto the thin alumina film at 60 K. (a) 0.003 ML Rh (1000 Å × 1000 Å, $U_{sample} = 4.0$ V, I = 0.07 nA). (b) 0.006 ML Pd (2000 Å × 2000 Å, $U_{sample} = 3.0$ V, $I = 0.08$ nA). The line protrusions are domain boundaries of the oxide film.

high infrared absorption cross section. In this way, very low particle concentrations may be studied by infrared spectroscopy, providing access to extremely small particle sizes ranging down to single, isolated metal atoms. When the as-deposited metal aggregates are exposed to CO, uniform and structurally well-defined surface carbonyl complexes are formed. They give rise to characteristic, sharp signatures in the infrared spectrum. Valuable and otherwise hardly accessible information on particle size and structure may hence be gained.

While large CO exposures result in the formation of CO-saturated complexes, by applying low gas exposures also complexes containing only a single CO molecule are accessible. The vibrational frequencies of such monocarbonyls formed from single metal atoms may be compared to those of neutral and charged MCO species in rare-gas matrices.[21−25] In this way, information on the charge state of single oxide-supported metal atoms may be extracted. Infrared spectroscopy therefore constitutes a means to approach a question that has been a constant matter of debate: the direction and extent of charge transfer at metal-ceramic interfaces.[26,27]

2. Experimental Section

Experiments were performed in a multi-chamber ultrahigh vacuum system with a base pressure below 2×10^{-10} mbar. The NiAl(110) crystal was mounted on a sample carrier which could be transferred between the various experimental stages. The crystal temperature was monitored by a NiCr/Ni thermocouple spot-welded to the sample.

STM images were taken with a variable temperature scanning tunneling microscope (Omicron). Because the sample transfer system between the preparation and infrared stage, on one hand, and the microscope, on the other hand, was not equipped with sample cooling facilities, the microscope was also operated at room temperature in this study. Infrared spectra were acquired with a vacuum infrared spectrometer (Bruker IFS 66v/S). A liquid nitrogen cooled MCT detector was used to detect the p-polarized light reflected from the sample surface at 84° grazing incidence. Typically, 1024 scans were accumulated, corresponding to an accumulation time of 160 s. The spectral resolution after apodization was 3.3 cm^{-1}.

The alumina film was prepared via oxidation of the NiAl(110) single-crystal surface;[28] its quality was checked by STM as well as via its phonon bands in the infrared spectrum.

Metals (>99.9%) were evaporated from a rod via electron bombardment. During evaporation the sample was put on a retarding potential to avoid effects due to metal ions accelerated toward the sample. Flux calibration was performed with a quartz crystal microbalance as well as by two-dimensional submonolayer growth on NiAl(110) and subsequent STM measurements. Deposition rates varied between 0.02 and 0.45 monolayers (ML) per min (1 ML palladium, rhodium, and iridium correspond to 1.53, 1.60, and 1.57×10^{15} atoms cm^{-2}, respectively). The samples were exposed to CO (AGA, >99.997%) and ^{13}CO (Cambridge Isotope Laboratories, >99% ^{13}C, >90% ^{16}O) utilizing a pinhole doser. Surface saturation required doses of below 4 L (1 L = 1 langmuir = 10^{-6} Torr s).

3. Results and Discussion

To control the structure and size of oxide-supported metal particles, we have utilized nucleation and growth of vapor-deposited metal atoms under ultrahigh vacuum conditions. As a substrate, we have chosen a thin, well-ordered and atomically flat alumina film grown on a NiAl(110) single-crystal surface.[28,29]

In previous work on nucleation and growth of Pd, Rh, and Ir on this alumina film, three types of metal nucleation sites were identified: (a) line defects constituting the deepest potential wells for metal adatoms, most notably antiphase domain boundaries with characteristic distances of 100 to 200 Å, but also reflection domain boundaries and substrate steps;[30,31] (b) point defects[32,33] with a number density of about 10^{13} cm^{-2}; and (c) surface sites between the point defects, possibly regular oxide sites, exerting the weakest influence on the metal atoms.[33] The nucleation behavior of transition metals on the film is determined by the relation between the thermal energy of diffusing adatoms and the metal-oxide interaction strength at these nucleation centers. Therefore, to access very small particle sizes or even single metal atoms, low substrate temperatures and metal exposures are to be applied. For the metals under consideration in the present study, a rising metal-oxide interaction strength along the series Pd < Rh < Ir was found.[32−34] At 90 K, only few adatoms possess sufficient thermal energy to reach a line defect. Pd and Rh are trapped at the point defects, while Ir mostly nucleates between these defects.[32,33] At 60 K, Rh nucleates at surface sites between the point defects as well.[33,34] We shall see that this is most probably also the case for Pd.

Room-temperature STM images of extremely small Pd and Rh exposures deposited at 60 K are shown in Figure 1. Rh particles (Figure 1a) are mostly located inside the oxide domains.

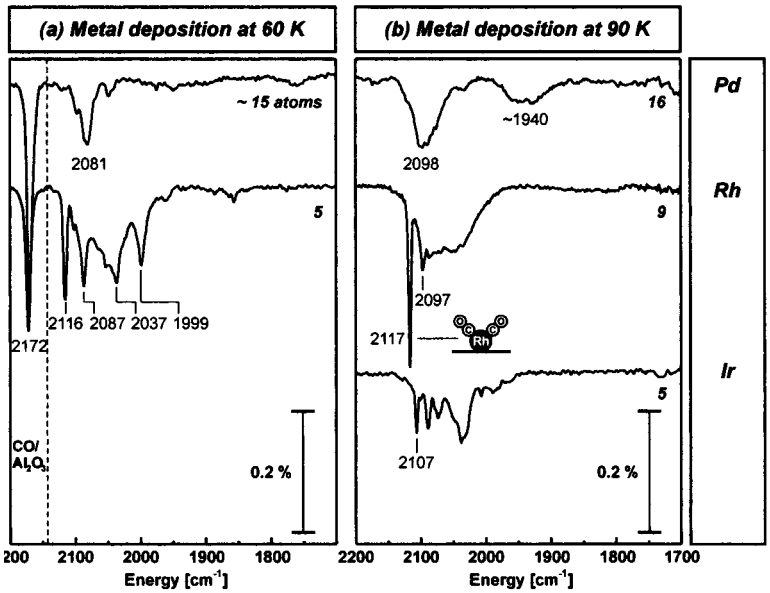

Figure 2. Infrared spectra taken after deposition of small amounts of (a) Pd and Rh at 60 K and of (b) Pd, Rh, and Ir at 90 K and subsequent saturation with CO. Metal deposition, gas dosage, and data acquisition were performed at the same temperature in each case. The average number of atoms per particle, as determined from room-temperature STM images of the deposits, is given next to the spectra.

Their average size is given by the ratio between the number density of Rh atoms deposited and the number density of aggregates visible in the STM image. It amounts to 3 to 4 Rh atoms. By contrast, the Pd aggregates (Figure 1b) contain 12 atoms on average. They partly decorate step edges and domain boundaries, which appear as protruding lines in the STM images. This finding seems to be at conflict with the description of the nucleation behavior given above. However, as we shall show below, the infrared spectra of CO adsorbed on Pd deposited at 60 K are characteristic of objects containing only a few atoms or even a single Pd atom. During heating of the samples to room temperature in order to perform STM measurements, thermally activated metal migration sets in, leading to an agglomeration of the Pd at the line defects. Small Rh aggregates prepared at 60 K only migrate to oxide point defects, while single Rh atoms initially trapped at such point defects diffuse to already existing aggregates.[33,35] Accordingly, the average particle sizes given in the following have to be taken as upper bounds for the particle sizes originally generated.

Therefore, it is clearly desirable to perform metal nucleation and growth experiments in the tunneling microscope while cooling the sample. Such experiments are under way.[36] Even under such conditions it may be a difficult task to image, e.g., metal dimers or trimers on insulator substrates with atomic resolution. As we shall see in the following, structural and electronic information on such ultrasmall aggregates may be obtained by IRAS.

3.1. Saturated Metal Deposits. Figure 2 shows infrared spectra of low Pd, Rh, and Ir exposures saturated with CO. Metal deposition, gas exposure, and data acquisition were performed (a) at 60 K and (b) at 90 K, respectively. The average numbers of atoms per metal particle as determined by room-temperature STM are given next to the spectra.

In the C−O stretching region, broad infrared bands as well as extremely narrow signals with halfwidths below 4 cm^{-1} are observed (Figure 2). We first discuss the kind of information inherent in such spectra, taking Rh as an example, and then move on to Pd and Ir.

Starting with *rhodium* deposited at 90 K (Figure 2b), the spectral weight is highest at frequencies above 1950 cm^{-1}. This points to predominantly terminally bound CO molecules. The spectrum is dominated by a sharp signal at a frequency of 2117 cm^{-1}, indicating structurally uniform, well-defined surface species. Their stoichiometry has been elucidated by taking infrared spectra of deposits saturated with isotopic CO mixtures. A splitting of the feature into three bands proves that Rh dicarbonyl species, $Rh(CO)_2$, are present.[33] They are located at the oxide point defects[33] and hence are formed from the atomic nuclei of heterogeneous Rh nucleation at these defects. Such a dicarbonyl possesses two C−O stretching modes, a symmetric and an antisymmetric mode. On the thin alumina film employed in the present study, only the symmetric mode of a bent dicarbonyl may be observed by infrared spectroscopy, since for thin oxide films on metal substrates the metal surface selection rule applies. We note that the symmetric stretching frequency of the Rh dicarbonyl species observed in the present study closely resembles that of $Rh(CO)_2$ on technical Rh/Al_2O_3 catalysts[37−43] (∼2100 cm^{-1}) and of $Rh(CO)_2$ on planar $TiO_2(110)$ surfaces[44] (2112 cm^{-1}).

As evidenced by infrared spectra recorded after successive annealing steps (Figure 3a), the Rh dicarbonyl is stable up to temperatures of 200 to 250 K. By contrast, the broad feature at lower frequencies is still present after heating to room temperature, albeit somewhat modified in shape. Like a corresponding band observed on technical Rh/Al_2O_3 catalysts,[37−43] it is due to CO on larger Rh particles.[34,35] The small signal at 2097 cm^{-1} will be discussed later, as infrared data from Rh deposits prepared at lower temperatures will aid in its assignment.

If the substrate temperature during Rh deposition and gas dosage is reduced to 60 K, a complex infrared spectrum with a number of sharp signals results (Figure 2a). At this temperature, submonolayer quantities of CO may physisorb on the alumina film itself.[45] These CO molecules give rise to an infrared band at 2172 cm^{-1}, which is also observed upon CO exposure of the pristine oxide film. Its comparatively low intensity at saturation shows that only a small fraction of alumina surface sites stabilizes CO at 60 K. These are most probably oxide defect sites.

The Rh dicarbonyl band at 2116 cm^{-1} is considerably reduced in intensity as compared to the 90 K deposit, showing that at

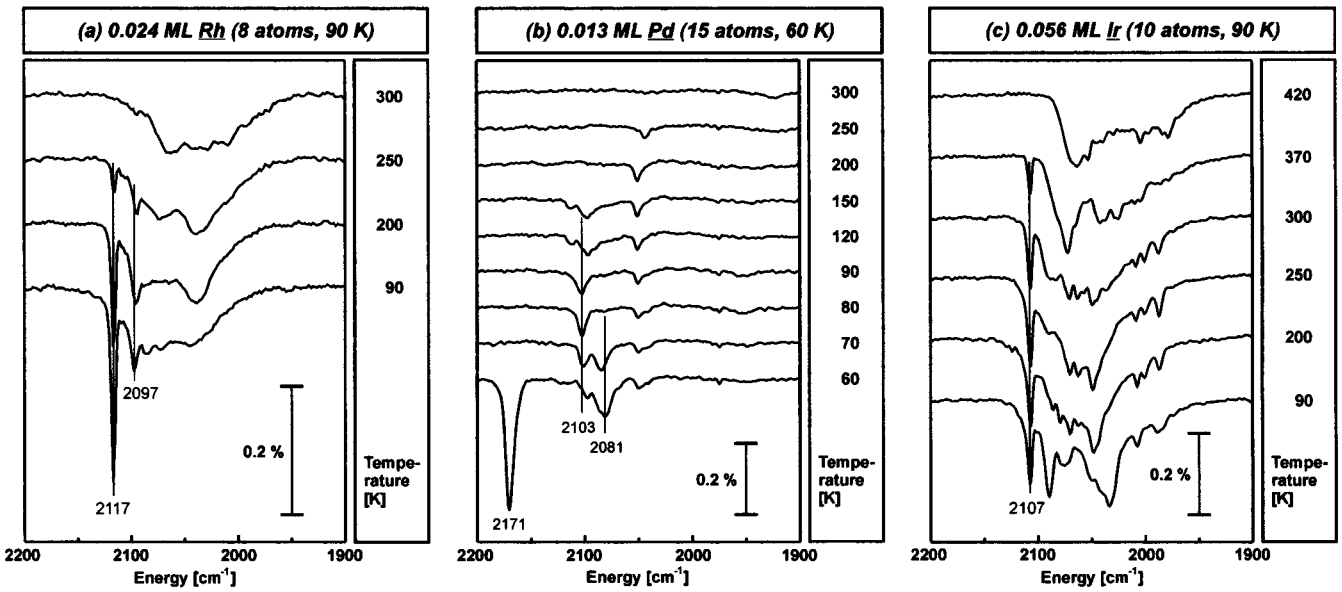

Figure 3. Infrared spectra taken after metal deposition and CO saturation at low temperature and after successive annealing steps to the temperatures given next to the spectra: (a) Rh, 90 K; (b) Pd, 60 K; (c) Ir, 90 K.

60 K less Rh atoms are trapped at the point defects. This is due to a lower metal atom diffusion length at reduced temperatures: the adatoms mostly nucleate between the point defects, possibly at regular oxide sites, before they can reach the defect sites. From these nuclei, different carbonyl species are formed, resulting in discrete infrared bands at 2087, 2037, and 1999 cm^{-1}. The difference in nucleation site is reflected in a low thermal stability of these carbonyls: their infrared features disappear on heating to temperatures between 80 and 150 K (not shown). Structural information on the surface complexes may again be gained from isotopic mixture experiments.[33] These indicate, e.g., that the species giving rise to the signal at 1999 cm^{-1} each contain only a single CO molecule, while the band at 2087 cm^{-1} originates from surface complexes containing three or more CO molecules.[33] We note that the C−O stretching frequency of 1999 cm^{-1} is lower than that of a free CO molecule[46] (2143 cm^{-1}) by 6.7%, in reasonable agreement with a frequency reduction of 7.7−8.6% found in a density functional theory (DFT) study of gas-phase Rh_n monocarbonyls.[47] DFT calculations of Rh carbonyls including an alumina support are under way.[48] They may enable a detailed structural assignment of the infrared bands observed in the present experimental study.

Finally, we would like to come back to the band at 2097 cm^{-1} observed after Rh growth at 90 K (Figures 2b and 3a). Its low halfwidth (as well as the lack of a wavenumber shift with rising CO exposure, see section 3.2) shows that also this signal originates from isolated, uniform surface species. Under conditions of lower metal diffusion length, i.e., after Rh deposition at 60 K, they are not formed (Figure 2a). Hence, they are most likely formed from metal nucleated at oxide defect sites. Concerning its stoichiometry, exposure to an isotopic CO mixture results in only one additional band,[33,34] consistent with a monocarbonyl. Its thermal stability is somewhat higher than that of Rh dicarbonyl at oxide point defects (Figure 3a), indicating a nucleation site involving a stronger metal-oxide interaction. We thus propose that the signal at 2097 cm^{-1} arises from a small quantity of RhCO, most probably formed from Rh atoms located at line defects.

Proceeding to *palladium* deposited at 90 K, nucleating at point defects,[32] broad C−O stretching features due to terminally bound (2098 cm^{-1}) and multiply coordinated (∼1940 cm^{-1}) molecules are observed (Figure 2b). Such broad signals with a large fraction of terminally bound CO are typical for adsorption on small, disordered Pd particles, as infrared data from technical Pd/Al_2O_3 catalysts[49−51] and corresponding planar model systems[52] show. Evidently, in the present case the Pd is less highly dispersed than the Rh discussed above, revealing a weaker tendency of Pd to nucleate at the point defects. Such infrared spectra from three-dimensional Pd aggregates on the alumina substrate under consideration are discussed in more detail elsewhere.[34,53]

After Pd growth at 60 K, the average particle size determined by room-temperature STM is essentially the same as at 90 K. Despite this, the infrared spectrum of adsorbed CO is significantly altered (Figure 2a). This supports the presumption that the nucleation behavior at 60 K differs from that at 90 K: a comparatively narrow signal at 2081 cm^{-1} suggests that uniform carbonyl species are present.[54] On annealing to 80 K, this infrared feature vanishes at the expense of a new signal at a higher frequency (Figure 3b). The Pd carbonyl species thus resemble the Rh carbonyls prepared at 60 K in their thermal instability. It is therefore likely that at 60 K also Pd nucleates at regular surface sites, forming extremely small aggregates or even single Pd atoms.

Finally turning to *iridium* nucleation at 90 K, we observe a spectral behavior reminiscent of Rh and Pd at 60 K (Figure 2b). This shows that, even at 90 K, Ir forms ultrasmall aggregates transformed to carbonyls by CO. Their thermal stability is low, except for the species giving rise to a band at 2107 cm^{-1} (Figure 3c). Even after annealing to 370 K, this signal is not greatly diminished. Adsorbing isotopic CO mixtures, it gives rise to a triplet of narrow bands (Figure 4a). One might suspect that the band at 2090 cm^{-1} observed for a mixture containing 25% ^{12}CO (Figure 4a, bottom) arises from the same surface complex as a signal from a pure ^{12}CO exposure at the same frequency. Its thermal behavior, however, is identical to the band at 2107 cm^{-1} (Figure 4b), proving that it is indeed part of a band triplet. The signal at 2107 cm^{-1} must therefore be due to the symmetric stretch of Ir dicarbonyl, $Ir(CO)_2$. Judging from its high thermal stability, even exceeding that of $Rh(CO)_2$ located at point defects, it is very likely that also $Ir(CO)_2$ originates from Ir atoms at such defect sites. As in the

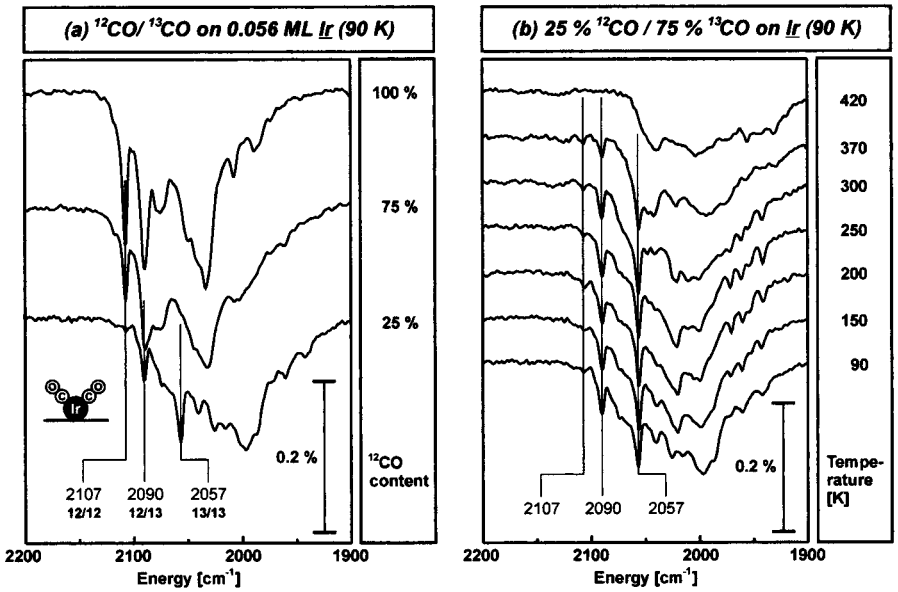

Figure 4. (a) Infrared spectra taken after deposition of 0.056 ML Ir at 90 K (average particle size as determined from room-temperature STM: 10 atoms) and subsequent saturation with different isotopic mixtures of ^{12}CO and ^{13}CO at the same temperature. (b) Infrared spectra taken after deposition of 0.056 ML Ir at 90 K and subsequent saturation with an isotopic mixture of 25% ^{12}CO and 75% ^{13}CO at the same temperature and after successive annealing steps to the temperatures given next to the spectra.

case of $Rh(CO)_2$, the symmetric stretching frequency of the Ir dicarbonyl species on our alumina model substrate is close to that of corresponding dicarbonyls on technical Ir/Al_2O_3 catalysts (2107−2090 cm^{-1}).[55]

Comparing our findings on metal nucleation on the alumina film, the tendency to form ultrasmall aggregates rises from Pd across Rh to Ir. This is consistent with a metal-oxide interaction strength increasing in the same order.[32−34]

3.2. Monocarbonyls. So far, we have concentrated on the vibrations of saturated CO adlayers. Now we will follow the spectral behavior as a function of gas exposure from zero upward, in other words, from bare metal nuclei across singly occupied metal atoms and particles up to saturation.

In Figure 5, series of infrared spectra of various metal deposits (Rh and Pd at 60 K, Rh and Ir at 90 K) are displayed as a function of CO exposure. Narrow signals appear, gain intensity at constant frequency and, in some cases, disappear again until saturation is reached. No continuous dipole shift with rising coverage is observed (except for the broad, structureless band due to larger Rh aggregates at 90 K). Such a blue shift would be expected if the CO coverage varied quasi-continuously, as is the case on larger metal aggregates.[34] By contrast, the discrete spectral evolution again confirms that all surface species contain only a small number of CO molecules and, hence, metal atoms and have a well-defined structure.

We now focus on the lowest CO exposures. For Pd grown at 60 K (Figure 5a), a single, narrow, and intense infrared signal at 2052 cm^{-1} is observed in this coverage regime. For Ir deposited at 90 K (Figure 5b), such a signal is located at 2006 cm^{-1}. When Rh is deposited at 90 K (Figure 5c), we find a band at 1994 cm^{-1}; for Rh grown at 60 K (Figure 5d), additional signals at 1966 cm^{-1} and 2000 cm^{-1} are observed. At such low CO exposures, it is expected that all spectral details are due to surface species containing only a single CO molecule, i.e., M_n-CO species. Isotopic mixture experiments confirm this expectation. Figure 6 exemplifies this for the case of an Ir deposit. After exposing the surface to small amounts of a mixture of ^{12}CO and ^{13}CO, only two sharp signals are observed, consisting of a ^{12}CO band at 2007 cm^{-1} and a ^{13}CO feature at 1958 cm^{-1}. This spectral behavior is characteristic for monocarbonyl species.

Singly occupied metal entities of different sizes may contribute to the spectra taken at low CO exposures. The observation of infrared features within a narrow frequency range for each metal indicates that the C−O stretching frequency of the monocarbonyls depends only weakly on the size of the metal center. This is in line with results from a DFT study of Rh_nCO species in the gas phase.[47] As discussed in conjunction with the infrared spectra taken upon CO saturation, the Rh deposits include a significant fraction of single metal atoms located at oxide point defects. This fraction is highest at 90 K. At low gas exposures, monocarbonyls formed from these single metal atoms, i.e., MCO species, will therefore contribute considerable spectral weight. This enables us to assign the intense C−O stretching signals observed at low gas exposures (Figure 5c) to such MCO, yielding a stretching frequency of 1994 cm^{-1} for RhCO located at oxide point defects.

At 60 K, aside from Rh at point defects also some of the homogeneously nucleated Rh might be monatomic. If this is the case, stretching frequencies of 1966 or 2000 cm^{-1} (Figure 5d) are due to RhCO at regular oxide sites. Similarly, the Ir deposits prepared at 90 K include isolated Ir atoms at point defects and perhaps at regular sites. The corresponding IrCO species exhibit a stretching frequency of 2006 cm^{-1} (Figure 5b). Also concerning Pd at 60 K, there is some evidence for the presence of atomically disperse metal at an unknown site (see section 3.1). The stretching signal at 2052 cm^{-1} (Figure 5a) may therefore be due to such PdCO.

In passing, we would like to comment on the surprisingly intense C−O stretching features at gas exposures around 0.05 to 0.1 L (Figure 5). This behavior may be rationalized by reverting to vibrational data of free $M_n(CO)_m$ obtained from DFT calculations. Such studies predict a pronounced dependence of the stretching intensity per CO on the composition of the carbonyl species as well as on their detailed geometric and electronic structure.[23,47,56] Notably, the C−O stretch of, e.g., RhCO is consistently found to be more intense than the symmetric stretch of bent $Rh(CO)_2$. A seemingly irregular intensity behavior with increasing CO coverage may result.

3.3. Metal Charge Probed by Vibrational Spectroscopy. The C−O stretching frequencies of MCO species are of special

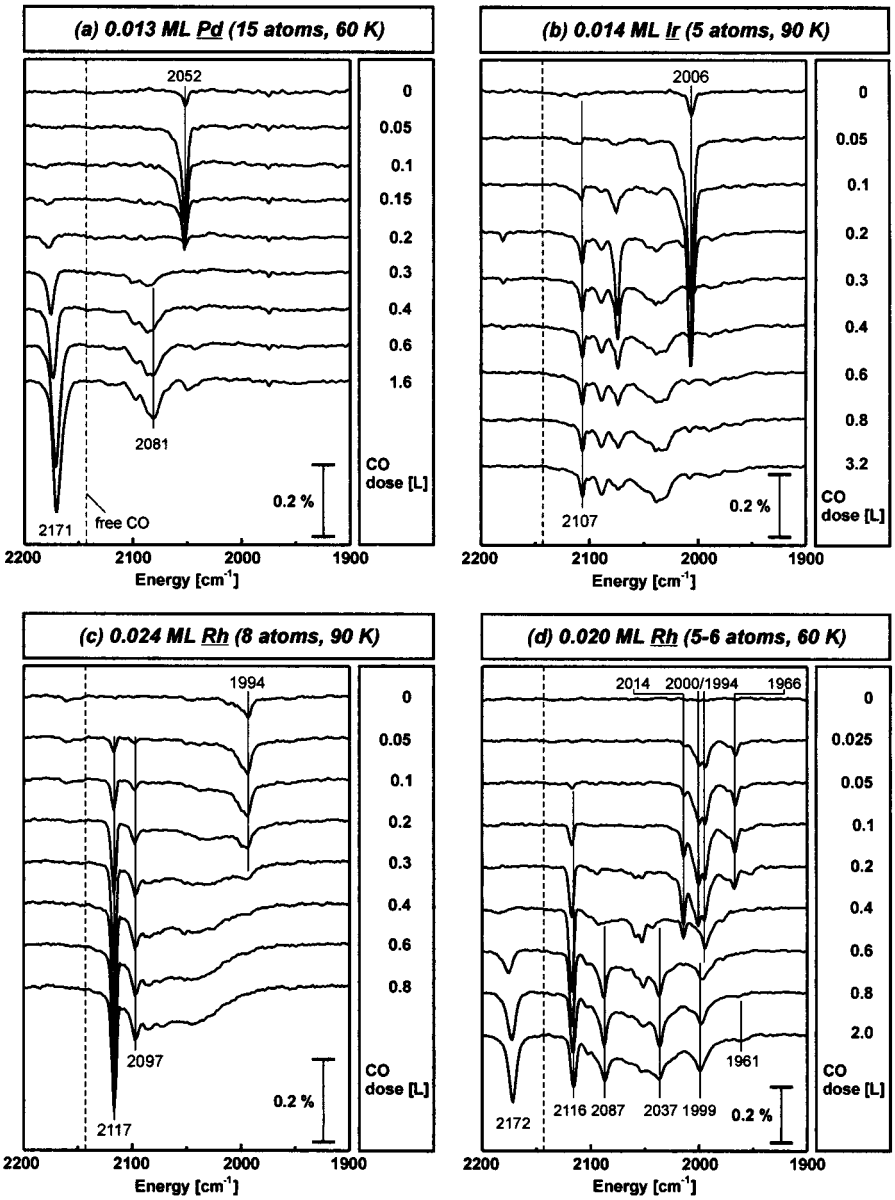

Figure 5. Infrared spectra taken after metal deposition and exposure to increasing CO doses at the same temperature: (a) Pd, 60 K; (b) Ir, 90 K; (c) Rh, 90 K; (d) Rh, 60 K. C−O stretching features detected on nominally clean surfaces are due to background gas adsorption during sample preparation. The stretching frequency of CO in the gas phase[46] (2143 cm^{-1}) is indicated by a dashed line. Due to the absence of any relevant features below 1900 cm^{-1} (only minority species, if at all), the lower frequency regime has been omitted in the spectra.

interest, as they may be compared to vibrational frequencies of corresponding compounds in rare gas matrices. In such weakly interacting media, both neutral[21−25] MCO and the singly charged[23−25] forms MCO^+ and MCO^- have been stabilized for M = Pd, Rh, and Ir. Their C−O stretching frequencies were found to depend sensitively on the charge of the species (Table 1), which may primarily be attributed to variations in the extent of metal-CO $2\pi^*$ back-donation.[56] The removal of one electron, giving MCO^+, increases the C−O stretching frequency by 133 to 152 cm^{-1}; an added electron, resulting in MCO^-, lowers this frequency by 147−194 cm^{-1}. These experimental findings are supported by DFT calculations (Table 1), predicting a blue shift from MCO to MCO^+ by 106 to 253 cm^{-1} and a red shift from MCO to MCO^- by 119 to 199 cm^{-1}.[22−25,47,56,57] While also the detailed electronic state of the metal atom affects the C−O stretching frequency,[23,24,47] this influence is clearly smaller than the charge dependence. Via the extent of metal-CO $2\pi^*$ back-donation, the C−O stretching frequency may thus be used as an indicator of charge on a metal center.

Infrared spectroscopy of adsorbed CO therefore constitutes a tool to study the extent of metal-oxide charge transfer. We note that a possible complication of such a quantification might arise from Pauli repulsion between the diffuse CO 5σ lone pair and occupied metal states.[58,59] The presence of an oxide substrate may alter the strength of the Pauli repulsion, leading to frequency shifts, even when no metal-oxide charge transfer occurs.[60] As it is a complex task to distinguish the contributions to the frequency shift, knowledge on such effects is still scarce. We will therefore assume that charge transfer is the main cause for variations of the C−O stretching frequency.

To establish a correct frequency−charge relationship, it has to be taken into account that the total charge of free or matrix-isolated MCO species is not necessarily identical to the charge localized on the metal atom. Yet, according to DFT calculations[22−25,56] the metal atom in neutral MCO is indeed close to neutral, being positively charged by only +0.1 to +0.2 elementary charges. In MCO^+, the charge state of the metal center ranges between +0.8 and +1.1, while for MCO^- values

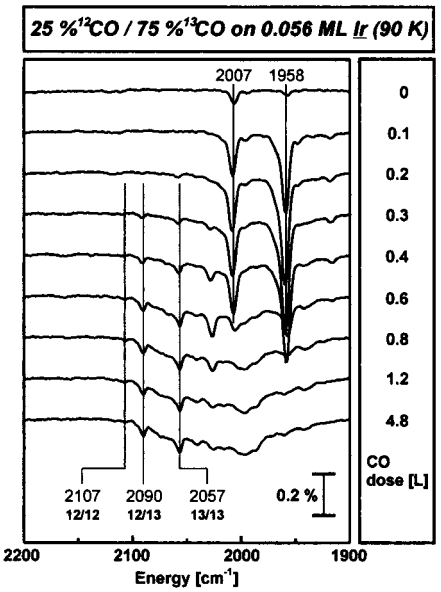

Figure 6. Infrared spectra taken after deposition of 0.056 ML Ir at 90 K (average particle size as determined from room-temperature STM: 10 atoms) and exposure to increasing doses of an isotopic mixture of 25% ^{12}CO and 75% ^{13}CO at the same temperature. C−O stretching features detected on the nominally clean surface are due to background gas adsorption during sample preparation.

TABLE 1: C−O Stretching Frequencies [cm^{-1}] of Neutral and Singly Charged MCO Species (M = Pd, Rh, and Ir) in Ne and Ar Matrices and According to DFT Calculations

	MCO^-	MCO	MCO^+	method	reference
Pd	1909	2056/2057	2206	Ne	(25)
		2044/2050		Ar	(22)
	1914	2113	2287	DFT	(25)
		2099	2224	DFT	(56)
Rh	1829	2023/2024	2174	Ne	(23,24)
		2008/2013		Ar	(21)
	1814	2008		Ar	(24)
	1823−1844	1956−2005	2129−2136	DFT	(23,24)
		2037	2202	DFT	(56)
	1888	2085	2252	DFT	(57)
		2043	2296	DFT	(47)
Ir	1843	2023/2025	2157	Ne	(24)
		2000		Ar	(21)
	1843−1866	2011−2022	2125−2128	DFT	(24)

from −0.5 up to −1.0 are usually found. We conclude that matrix isolated metal carbonyls represent valid calibration standards for infrared studies of surface carbonyl species.

As experimental data on vibrational frequencies of free MCO (M = Pd, Rh, and Ir) are not available, we revert to the matrix isolation data presented in Table 1. Among the rare gas matrices, vibrational frequencies of molecules in Ne matrices are generally closest to the gas-phase values.[61] This leads us to the following comparison of C−O stretching frequencies of MCO on the alumina substrate studied in this work and those of neutral, matrix-isolated MCO:[23−25]

PdCO in Ne matrix, 2056 cm^{-1}; on alumina (?), 2052 cm^{-1};

RhCO in Ne matrix, 2023 cm^{-1}; at alumina point defects, 1994 cm^{-1}; at regular sites (?), 1966 or 2000 cm^{-1};

IrCO in Ne matrix, 2025 cm^{-1}; at alumina point defects and perhaps at regular sites, 2006 cm^{-1}.

The frequencies of the surface species are only slightly lower than those of their neutral matrix isolated counterparts. Taking into account that the charge localized on the metal centers of the latter amounts to +0.1 to +0.2, we conclude that the charge state of the metal atoms on the oxide surface is very close to neutral, lying between −0.2 and +0.2. We have, therefore, no indication of any significant metal-oxide charge transfer.

By contrast, the RhCO band at 2097 cm^{-1}, which most probably originates from Rh trapped at oxide line defects, is red shifted with respect to the neutral RhCO in Ne by 74 cm^{-1}. This indicates a charged Rh center. From the size of the shift, a charge on the Rh atom of +0.6 to +0.7 may be estimated. The strong metal-oxide interaction at the line defects thus appears to be connected with a significant extent of metal oxidation.

Finally, we would like to note that in principle the C−O stretching frequencies of metal dicarbonyls, $M(CO)_2$, likewise carry information on the charge of the metal center. In fact, the observed[23−25] and calculated[23−25,56,57] charge-induced frequency shifts of free and matrix-isolated dicarbonyls are similar to those of the monocarbonyls discussed above. But the vibrational frequencies may also depend strongly on the C−M−C bond angle[23,24] which varies with the environment of the $M(CO)_2$ species, ranging from about 90° on technical catalysts[38,39] to 180° for some matrix-isolated dicarbonyls[23,24] In our system, the observed $M(CO)_2$ species are certainly bent (due to the metal surface selection rule, both their symmetric and their antisymmetric C−O stretching vibrations would otherwise be unobservable), however with an unknown C−M−C bond angle. Furthermore, little is known about the functional relationship between frequency and bond angle. We therefore do not attempt to utilize infrared data of our dicarbonyl species to quantify charges.

4. Summary and Conclusion

To establish relationships between structure, electronic properties, and reactivity of small metal particles, detailed information on particle size and structure at the atomic level is essential. There is, however, no powerful experimental tool to provide such data. In this work, we have demonstrated the potential of infrared spectroscopy to elucidate atomic details of ultrasmall oxide-supported aggregates. Adsorbed CO gives rise to discrete, sharp signatures in the infrared spectra. Adsorption of such probe molecules on larger particles results in broad absorption bands.

We have shown that, following this approach, atomic nuclei of metal growth on an alumina model substrate may be detected. Upon CO saturation of such single Rh and Ir adatoms located at oxide point defects, dicarbonyl species, $Rh(CO)_2$ and $Ir(CO)_2$, are formed. Their symmetric stretching frequencies are very close to those of corresponding dicarbonyls on technical catalysts. The detection of single adatoms by infrared spectroscopy opens up possibilities to study, e.g., the thermal behavior of such nuclei and the carbonyls formed from them. But also information on larger carbonyl species present between the point defects, probably at regular oxide sites, may be extracted from the infrared spectra by isotopic mixture experiments. On our alumina substrate, their thermal stability is very low.

Applying small gas exposures, monocarbonyls are formed. In this way, the regime of singly occupied metal particles may be explored. Singly occupied individual metal atoms, i.e., MCO species, are of special interest, as their C−O stretching frequencies may be compared to those of neutral and charged MCO species isolated in rare-gas matrices. Assuming that Pauli repulsion between the diffuse CO 5σ lone pair and occupied metal states does not differ substantially between matrix-isolated and oxide-supported MCO, this provides access to the extent of metal-oxide charge transfer. The frequencies of the monocarbonyls RhCO, IrCO, and possibly also of PdCO, located at

regular sites or point defects of the oxide film are close to those of their neutral matrix-isolated counterparts. The data yield metal charges between −0.2 and +0.2, i.e., there is little metal-oxide charge transfer. By contrast, the stronger metal-oxide bond between single Rh atoms and oxide line defects is connected with a significant extent of metal oxidation, corresponding to the transfer of 0.5 to 0.6 elementary charges to the alumina substrate.

These considerations should equally well be transferable to other metal-on-insulator systems and technical catalysts. We have thus shown that infrared spectroscopy may contribute to the elucidation of structure and charge of ultrasmall supported metal aggregates with sizes down to a single atom.

Acknowledgment. For financial support of our work, we are grateful to a number of agencies: Deutsche Forschungsgemeinschaft (DFG), Bundesministerium für Bildung und Forschung (BMBF), and Fonds der Chemischen Industrie. This work has also been supported by Synetix, a member of the ICI group, through their Strategic Research Fund. M.F. thanks the Studienstiftung des deutschen Volkes for a fellowship. Finally, we would like to thank Dr. T. Mineva, Professor N. Russo, and Professor G. Pacchioni for valuable discussions.

References and Notes

(1) Cox A. J.; Louderback J. G.; Bloomfield L. A. *Phys. Rev. Lett.* **1993**, *71*, 923.
(2) Haruta M. *Catal. Today* **1997**, *36*, 153.
(3) Freund H.-J. *Surf. Sci.* **2001**, *500*. In press.
(4) Heiz U.; Sanchez A.; Abbet S.; Schneider W.-D. *J. Am. Chem. Soc.* **1999**, *121*, 3214.
(5) Heiz U.; Schneider W.-D. *J. Phys. D: Appl. Phys.* **2000**, *33*, R85.
(6) Dayte A. K.; Smith D. J. *Catal. Rev.−Sci. Eng.* **1992**, *34*, 129.
(7) Bergeret G.; Gallezot P. In *Catalyst Characterization: Physical Techniques for Solid Materials*; Imelik B., Vedrine J. C., Eds.; Plenum Press: New York, 1994; Chapter 15.
(8) Bart, J. C. J.; Vlaic, G. *Adv. Catal.* **1987**, *35*, 1.
(9) Woodruff D. P.; Delchar T. A. *Modern Techniques of Surface Science*, 2nd ed.; Cambridge University Press: Cambridge, 1994.
(10) Chen C. J. *Introduction to Scanning Tunneling Microscopy*; Oxford University Press: New York, Oxford, 1993.
(11) Berkó A.; Ménesi G.; Solymosi F. *Surf. Sci.* **1997**, *372*, 202.
(12) Murray P. W.; Shen J.; Condon N. G.; Pang S. J.; Thornton G. *Surf. Sci.* **1997**, *380*, L455.
(13) Bonnell D. A. *Prog. Surf. Sci.* **1998**, *57*, 187.
(14) Lai X.; St. Clair T. P.; Valden M.; Goodman D. W. *Prog. Surf. Sci.* **1998**, *59*, 25.
(15) Dulub O.; Hebenstreit W.; Diebold U. *Phys. Rev. Lett.* **2000**, *84*, 3646.
(16) Xu C.; Lai X.; Zajac G. W.; Goodman D. W. *Phys. Rev. B* **1997**, *56*, 13464.
(17) Goodman D. W. *Surf. Rev. Lett.* **1995**, *2*, 9.
(18) Freund H.-J. *Angew. Chem., Int. Ed. Engl.* **1997**, *36*, 452.
(19) Bäumer M.; Freund H.-J. Prog. *Surf. Sci.* **1999**, *61*, 127.
(20) Hansen K. H.; Worren T.; Stempel S.; Lægsgaard E.; Bäumer M.; Freund H.-J.; Besenbacher F.; Stensgaard I. *Phys. Rev. Lett.* **1999**, *83*, 4120.
(21) Ozin G. A.; Hanlan A. J. L. *Inorg. Chem.* **1979**, *18*, 2091.
(22) Tremblay B.; Manceron L. *Chem. Phys.* **1999**, *250*, 187.
(23) Zhou M.; Andrews L. *J. Am. Chem. Soc.* **1999**, *121*, 9171.
(24) Zhou M.; Andrews L. *J. Phys. Chem. A* **1999**, *103*, 7773.
(25) Liang B.; Zhou M.; Andrews L. *J. Phys. Chem. A* **2000**, *104*, 3905.
(26) Finnis M. W. *J. Phys.: Condens. Matter* **1996**, *8*, 5811.
(27) Campbell C. T. *Surf. Sci. Rep.* **1997**, *27*, 1.
(28) Jaeger R. M.; Kuhlenbeck H.; Freund H.-J.; Wuttig M.; Hoffmann W.; Franchy R.; Ibach H. *Surf. Sci.* **1991**, *259*, 235.
(29) Libuda J.; Winkelmann F.; Bäumer M.; Freund H.-J.; Bertrams Th.; Neddermeyer H.; Müller K. *Surf. Sci.* **1994**, *318*, 61.
(30) Bäumer M.; Libuda J.; Sandell A.; Freund H.-J.; Graw G.; Bertrams Th.; Neddermeyer H. *Ber. Bunsen-Ges. Phys. Chem.* **1995**, *99*, 1381.
(31) Bäumer M.; Frank M.; Libuda J.; Stempel S.; Freund H.-J. *Surf. Sci.* **1997**, *391*, 204.
(32) Bäumer M.; Frank M.; Heemeier M.; Kühnemuth R.; Stempel S.; Freund H.-J. *Surf. Sci.* **2000**, *454−456*, 957.
(33) Frank M.; Kühnemuth R.; Bäumer M.; Freund H.-J. *Surf. Sci.* **2000**, *454−456*, 968.
(34) Frank M.; Bäumer M. *Phys. Chem. Chem. Phys.* **2000**, *2*, 3723.
(35) Frank M.; Kühnemuth R.; Bäumer M.; Freund H.-J. *Surf. Sci.* **1999**, *427−428*, 288.
(36) Magg N.; Giorgi J.; Bäumer M.; Freund H.-J. To be published.
(37) Yang A. C.; Garland C. W. *J. Phys. Chem.* **1957**, *61*, 1504.
(38) Yates, Jr., J. T.; Duncan T. M.; Worley S. D.; Vaughan R. W. *J. Chem. Phys.* **1979**, *70*, 1219.
(39) Rice C. A.; Worley S. D.; Curtis C. W.; Guin J. A.; Tarrer A. R. *J. Chem. Phys.* **1981**, *74*, 6487.
(40) Solymosi F.; Pásztor M. *J. Phys. Chem.* **1985**, *89*, 4789.
(41) Basu P.; Panayotov D.; Yates, J. T., Jr. *J. Phys. Chem.* **1987**, *91*, 3133.
(42) Solymosi F.; Knözinger H. *J. Chem. Soc., Faraday Trans.* **1990**, *86*, 389.
(43) Solymosi F.; Bánsági T. *J. Phys. Chem.* **1993**, *97*, 10133.
(44) Hayden B. E.; King A.; Newton M. A. *Chem. Phys. Lett.* **1997**, *269*, 485.
(45) Jaeger R. M.; Libuda J.; Bäumer M.; Homann K.; Kuhlenbeck H.; Freund H.-J. *J. Electron Spectrosc. Relat. Phenom.* **1993**, *64/65*, 217.
(46) Herzberg G. *Molecular Spectra and Molecular Structure*, 2nd ed.; Van Nostrand Reinhold: New York, 1950; Vol. I.
(47) Mineva T.; Russo N.; Freund H.-J. *J. Phys. Chem. A* Submitted for publication.
(48) Mineva T.; Russo N.; Freund H.-J., In preparation.
(49) Hicks R. F.; Qi H.; Kooh A. B.; Fischel L. B. *J. Catal.* **1990**, *124*, 488.
(50) Tessier D.; Rakai A.; Bozon-Verduraz F. *J. Chem. Soc., Faraday Trans.* **1992**, *88*, 741.
(51) Dulaurent O.; Chandes K.; Bouly C.; Bianchi D. *J. Catal.* **1999**, *188*, 237.
(52) Rainer D. R.; Wu M.-C.; Mahon D. I.; Goodman D. W. *J. Vac. Sci. Technol. A* **1996**, *14*, 1184.
(53) Wolter K.; Seiferth O.; Kuhlenbeck H.; Bäumer M.; Freund H.-J. *Surf. Sci.* **1998**, *399*, 190.
(54) The small feature at ∼2050 cm^{-1} probably originates from CO adsorbed on unoxidized NiAl patches.
(55) Solymosi F.; Novák É.; Molnár A. *J. Phys. Chem.* **1990**, *94*, 7250.
(56) Pápai I.; Goursot A.; St-Amant A.; Salahub D. R. *Theor. Chim. Acta* **1992**, *84*, 217.
(57) McKee M. L.; Worley S. D. *J. Phys. Chem. A* **1997**, *101*, 5600.
(58) Bagus, P. S.; Pacchioni, G. *Surf. Sci.* **1990**, *236*, 233.
(59) Curulla D.; Clotet A.; Ricart J. M.; Illas F. *J. Phys. Chem. B* **1999**, *103*, 5246.
(60) Bredow T.; Pacchioni G. *Surf. Sci.* **1999**, *426*, 106.
(61) Jacox M. E. *Chem. Phys.* **1994**, *189*, 149.